Journal of Hydrology: Regional Studies 38 (2021) 100968

Contents lists available at ScienceDirect

Journal of Hydrology: Regional Studies

journal homepage: www.elsevier.com/locate/ejrh

Quantifying changes and drivers of runoff in the Kaidu River Basin associated with plausible climate scenarios

Bingqian Zhao [a], Huaiwei Sun [a,*], Dong Yan [a], Guanghui Wei [b], Ye Tuo [c], Wenxin Zhang [d,e,*]

[a] School of Civil and Hydraulic Engineering, Huazhong University of Science and Technology, Wuhan 430074, China
[b] Tarim River Basin Management Bureau, Korla 841000, China
[c] Chair of Hydrology and River Basin Management, Technical University of Munich, Arcisstrasse 21, 80333 Munich, Germany
[d] Department of Physical Geography and Ecosystem Science, Lund University, Sölvegatan 12, 22362 Lund, Sweden
[e] Center for Permafrost (CENPERM), Department of Geosciences and Natural Resource Management, University of Copenhagen, Øster Voldgade 10, 1350 Copenhagen, Denmark

ARTICLE INFO

Keywords:
Snowmelt timing
ISIMIP2b
Tarim River Basin
Hydrological modeling
China

ABSTRACT

Study region: The Kaidu River Basin (KRB) is located on the central southern slope of the Tianshan Mountain in Northwest China.

Study focus: This work aimed to assess changes and main drivers of snowmelt-driven runoff in KRB associated with three future climate scenarios. Six versions of the "Cemaneige" snowmelt module embedded in the hydrological model "GR4J" were calibrated and evaluated. The bias-corrected climate datasets from CMIP5 Models were used to drive the optimal snowmelt-hydrological model for runoff prediction. The factors that lead to runoff variations were also assessed.

New hydrological insights: The significant declining trends of runoff were only predicted in the RCP4.5 and RCP8.5 scenarios. The declining trends of runoff were found in all the seasons. For the annual and summer runoff, compared to the historical period, both the RCP2.6 and RCP 4.5 periods showed a decline in the mid-century and a rise in the end-century; however, RCP8.5 showed a continuous decline during this period. Precipitation and evapotranspiration were ranked as the two most important factors regulating future runoff variations in all RCPs. In contrast, snowmelt timing is the second factor in the historical period, and its importance decreases in the warmer RCP scenarios. These results highlighted that the importance of snowmelt and snowmelt timing to the future runoff depends on the runoff responses to the trajectory of future changes in temperature and precipitation.

1. Introduction

Climate change may affect the atmospheric and surface radiation budget and thus alter variabilities of the global hydrological cycle, potentially increasing the risk of hydrological hazards (Pachauri et al., 2014; Alfieri et al., 2015). In addition, continuous global warming will likely redistribute precipitation and water resources between regions according to climate, topography, land cover type,

* Corresponding author.
* Corresponding author at: Department of Physical Geography and Ecosystem Science, Lund University, Sölvegatan 12, 22362 Lund, Sweden.
E-mail addresses: huaiweisun@whu.edu.cn (H. Sun), wenxin.zhang@nateko.lu.se (W. Zhang).

https://doi.org/10.1016/j.ejrh.2021.100968
Received 9 July 2021; Received in revised form 30 October 2021; Accepted 5 November 2021
Available online 17 November 2021

and human management of water resources (Chen (2014). As an essential component in the hydrological cycle, runoff may respond to climate change via its impact on water resource availability and distribution (Yuan et al., 2015; Azmat et al., 2018; Jahandideh-Tehrani et al., 2019). Experimental data-based evidence has demonstrated that global warming may intensify the global hydrological cycle, leading to an increase in global continental runoff (Labat et al., 2004). Floods in many tributary regions, like the Tarim River Basin, were found amplified at annual and seasonal scales after the 1980s, and their amplification was associated with the occurrence of rainstorms, glacier- and snowmelt, and climatic warming (Zhang et al., 2016a, 2016b; Gu et al., 2016, 2017; Sun et al., 2016). Therefore, the assessment of seasonal and inter-annual variations of runoff under climate change is vital for water resources provision that sustains ecosystem function and services and human social-economic developments (Deng et al., 2015; Zhu et al., 2017; Pradhanang et al., 2013).

Snowmelt is one of the primary sources of river runoff in the alpine regions. A robust estimate of snowmelt-driven runoff is critical to alpine flood forecasting, drought control, and other aspects associated with water resource planning (Zhang et al., 2006; Coppola et al., 2018). As warmer spring may lead to earlier snowmelt, a combination of snowmelt and extreme precipitation can easily cause flooding (Sun et al., 2018; Zhang et al., 2006). Therefore, snowmelt-driven runoff is particularly sensitive to climate change (Kundzewicz et al., 2015; Zhang et al., 2014a, 2014b). The challenge in predicting snowmelt-driven runoff is to understand the underlying causes of snowmelt and its relationship with the catchment water balance (Mccabe and Clark, 2005; Zampieri et al., 2015). Dahri et al. (2021) employed the Variable Infiltration Capacity (VIC) macroscale Hydrologic Model to simulate runoff based on snowmelt and precipitation in the high-altitude Indus River Basin. They pointed out that the improvement of input temperature and precipitation data is critical to obtaining robust simulations. As temperature is one of the controlling factors that determine the timing and magnitude of snowmelt and runoff (Zhang et al., 2006; Zhang et al., 2016; Fang et al., 2018), the degree-day model based on the temperature threshold, degree-day factor, and radiation coefficient could get comparable accuracies as energy balance models for simulating snowmelt but with less demand of input data (Liu et al., 2017; Troin et al., 2018). The GR4J model, a daily lumped rainfall-runoff model, has been widely applied to simulate catchment hydrology due to its simple four-parameter structure. Compared to the GR3J model, the GR4J model showed improved performance, particularly in simulating low flows (Edijatno et al. 1999; Perrin et al. 2003). Valéry et al. (2014a, 2014b) presented a comparison of six snowmelt models associated with two hydrological models, GR4J and HBV, and concluded that the most complex model did not yield the best performance in simulating runoff. Many snowmelt models, such as Cemaneige (Valéry et al., 2010), MOHYSE (Fortin and Turcotte, 2007), HYDROTEL (Turcotte et al., 2007), etc., have been developed to explore the relationship between snowmelt and runoff.

Climate change may cause significant impacts on water flow and water resources in the arid and semi-arid regions in Northwest China (Sun et al., 2015; Bao et al., 2017; Santos et al., 2019). The Tianshan Mountain, known as the water tower of Central Asia, is an important freshwater resource in China and a major source of rivers in Northwest China (Chen et al., 2016; Sorg et al., 2012; Wang et al., 2019). The Kaidu River Basin, one of four headwaters of the Tarim River Basin, is located on the southern slope of Tianshan Mountain and connects the Bayanbulak Swan Lake and finally flows into the Bosten Lake. The Kaidu River bears the important task of water transport to the lower reaches of the Tarim River (Chen et al., 2017). However, runoff of the four river basins that are situated in the south of Tianshan Mountain showed distinct responses to precipitation and temperature. Runoff in the Kaidu River Basin and the Huangshuigou Basin was co-regulated by both precipitation and temperature, which, however, were the dominant factor for regulating runoff in the Toxkon Basin and Kunmalik Basin, respectively. Shen et al. (2018) and Luo et al. (2017) have found that river streamflow was more sensitive to temperature change than precipitation change in Hotan River Basin, and the model structure strongly affected the hydrological response of climate change.

Robust projection of hydrological responses can help achieve sustainable social-economic development. An effective climate change adaptation strategy can be discovered by predicting runoff under future climate warming scenarios associated with different Representative Concentration Pathways (RCPs). Climate scenario projections are often used to drive hydrological models to quantify the future climate change impact on the watershed runoff. In this study, we aim to estimate future changes in seasonal and inter-annual runoff under the 21st century RCP scenarios and investigate the principal climate factors that regulate the trends and variability of runoff based on an optimized snowmelt-streamflow model. Four climate models from Phase 2b of The Inter-Sectoral Impact Model Intercomparison Project (ISIMIP2b; Frieler et al., 2017) were selected, and these climate projections have been bias-corrected using historical observational datasets. We chose three RCP scenarios to predict future runoff: RCP2.6, controlling global average temperature rise below 2 ℃; RCP4.5, forcing the climate system with steady radiation artificially; and RCP8.5, which has no climate change policy (van Vuuren et al., 2011; Thomson et al., 2011; Riahi et al., 2011). Accordingly, this study mainly addresses the following research questions: (a) How can we improve a combined snowmelt and streamflow model to simulate runoff of the Kaidu River Basin? (b) What are the impacts of three RCP scenarios on inter-annual and seasonal variations of runoff? (c) What are the major climate-related factors that control the trend and variability of future runoff, and how does their relative importance vary across different RCP scenarios?

2. Materials and methods

2.1. Study Area

The Kaidu River Basin is situated on the central southern slope of the Tianshan Mountain in Northwest China, bordering the Tarim Basin in the south. The entire river basin is enclosed between a longitude of 82°58′−86°05′E and a latitude of 42°14′−43°21′N, comprising an area of 19,012 km^2 above the Dashankou Hydrological Station (Fig. 1). The elevation for the bottom of the basin ranges from 2304 to 2565 m above sea level. The terrain is flat, surrounded by mountains with an altitude of 3928–4794 m. As the basin is

located in the hinterland of The Eurasian continent, far from the sea, close to the Taklamakan Desert, its climate type is continental temperate arid. However, due to its topographical characteristics, compared with the surrounding areas, the temperature is lower, and the precipitation is higher in the basin. The annual mean temperature is -1.82 ± 0.61 ℃, and the annual total precipitation is 328.8 ± 31 mm during 1961–2005. Precipitation shows a distinct seasonal pattern with spring of 44.7 mm and summer of 127.1 mm. The runoff of the Kaidu River comes from snow- and icemelt and rainfall. The accumulation of snow begins in November and ends in March of the following year. With the increase of temperature in April and May, seasonal snowmelt supplies rivers. The snowmelt-induced floods are commonly found in this region, such as the spring flood on April 24, 2011, exceeding the summer flood. In summer, the mountain snowmelt and rainfall are the main sources of the river.

2.2. Data sources

2.2.1. Meteorological and hydrological data sets for model calibration

To calibrate the hydrological model, the meteorological and hydrological observation data sets were used. The daily precipitation and temperature observations during 1961–2011 used the CN05.1 gridded observation data set with a resolution of $0.25^\circ \times 0.25^\circ$. This dataset was generated by interpolating the field data at more than 2400 stations across China using the approaches of ANUSPLIN (the Australian National University Spline) and ADW (Angular Distance Weighting), respectively (Wu and Gao, 2013). Because the basin was divided into three sub-basins through Archydro Tools in ArcGIS and two meteorological stations in the basin could not meet the data needs of the three sub-basins, we decided to use the CN05.1 gridded data set as the model climate input. The daily radiation used the net radiation data set from the NASA Global Land Data Assessment System (GLADS)– 2.0 dataset (https://disc.gsfc.nasa.gov), which was estimated from cloud and snow product combined with the algorithm by the Air Force Weather Agency AGRicultural METeorological modeling system (AGRMET). The hydrological data used the daily observed runoff data of the Dashankou Hydrological Station from 2005 to 2011, located at the outlet of the basin (Fig. 1).

2.2.2. Climate scenario data sets

Historical (1961–2005) and future (2006–2099) climate scenario data sets at daily temporal and 0.5° horizontal resolution from the Inter-Sectoral Impact Model Intercomparison Project project (ISIMIP2b) (Frieler et al., 2017) were used to run scenario simulations based on the optimized model. These climate scenario data sets consist of the Coupled Model Intercomparison Project (CMIP-5; Taylor

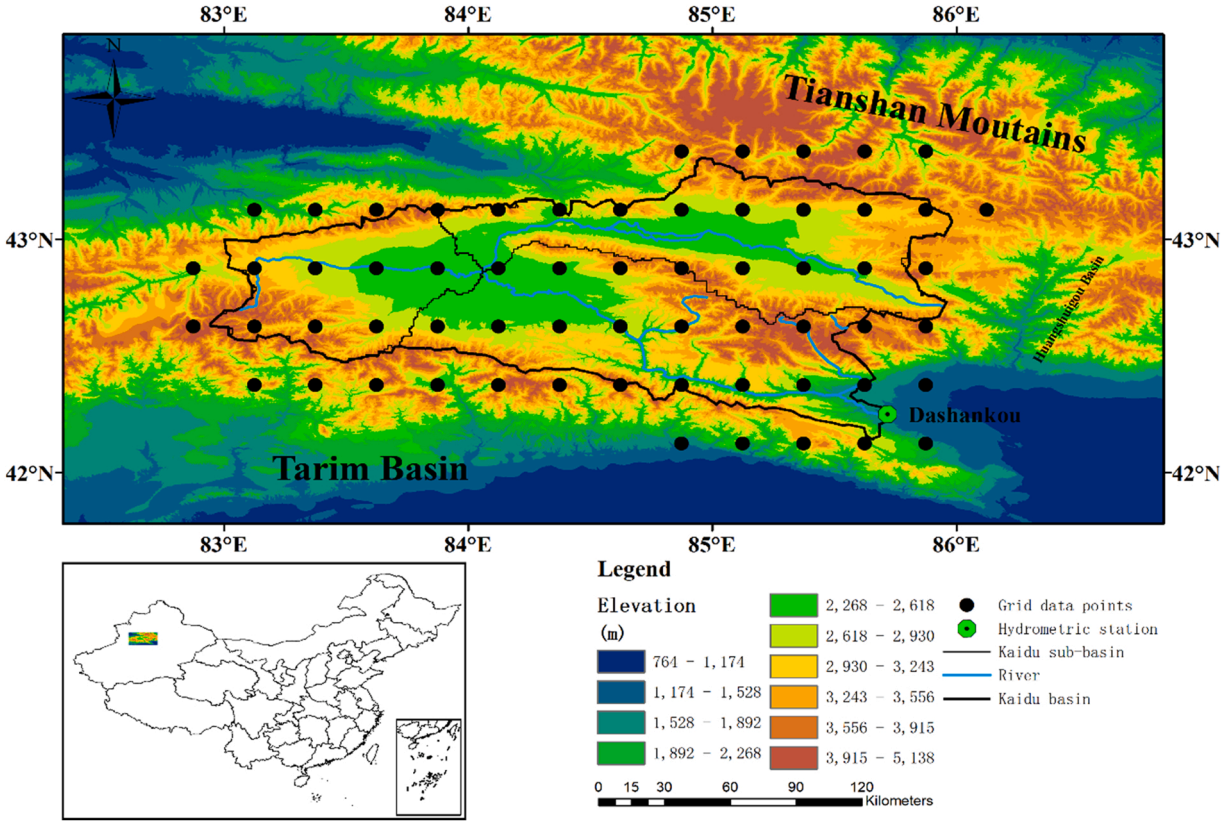

Fig. 1. Location of the Kaidu River Basin in Xinjiang, China. The black dots show the grid point extracted from the climate observation dataset (CN05.1; Wu and Gao, 2013), and the green dot indicates the Dashankou hydrological station.

et al., 2012) outputs from four Global Climate Models (GDFL-ESM2M, HADGEM2-ES, IPSL-CM5A-LR, MIROC5, shortened as GDFL, HADGEM2, IPSL, MIROC5) for low-to-high warming scenarios, i.e., the Representative Concentration Pathway (RCP) 2.6, RCP4.5, and RCP8.5 (Moss et al., 2010). Even though only four GCMSs may not be sufficient to represent the entire spread of regional climate change projected by the CMIP5 ensemble, we still note that for the China region, only one CMIP5 model projection is out of the range spanning across the four GCMs we selected (Frieler et al., 2017). To ensure the ISIMIP2b historical climate data sets consistent with the CN05.1 data set in the trends and variabilities of temperature and precipitation, a bias correction (see Section 2.4) for temperature and precipitation based on the CN05.1 data set was done for the ISIMIP2b historical climate datasets for the study area.

2.3. Runoff simulation

The hydrological model GR4J and the snowmelt module Cemaneige have been successfully applied to simulate runoff in mountainous areas, which can meet the needs of our study (Valéry et al., (2010; Troin et al., 2018; Arsenault et al. (2018. A brief description of the snowmelt module Cemaneige and the hydrological model GR4J model are given below.

2.3.1. Snowmelt module

The Cemaneige module simulates snow accumulation and melts using a snowpack to represent snow storage (snow water equivalent) and the thermal state of the snow. The snow storage can be added with the solid fraction of the precipitation. The thermal state of the snowpack determines the onset of the snowmelt. After calculation of the snow storage and thermal state, the potential snowmelt can be determined using the degree-day method. Finally, the actual snowmelt is the multiplication of the areal fraction of snow cover and the potential snowmelt.

Two critical hydrological processes related to snowmelt, rain/snow division, and snowmelt computation, were tested in this study to get a robust simulation of snowmelt runoff. As there are two different functions of rain/snow division and three different methods of snowmelt computation available in the Cemaneige module, six combinations of these functions (Table 1) had been coupled into the hydrological model to identify the optimized model, which was used in the future projection of snowmelt runoff.

2.3.1.1. Rain/snow division functions. Both single temperature threshold (Yang et al., 1997) and double temperature threshold (Wigmosta et al. (1994; Fuchs et al., 2001) functions are considered. The equations for these functions are as follows:

a) Single threshold function(STT)

$$S_p = \begin{cases} 1 & T_{mean} \le T_0 \\ 0 & T_0 \le T_{mean} \end{cases} \quad (1)$$

where S_p is the percentage of solids in precipitation, T_0 is a threshold temperature value (°C), and T_{mean} is the mean air temperature (°C).

b) Double threshold function(DTT)

$$S_p = \begin{cases} 1 & T_{mean} \le T_{snow} \\ (T_{mean}\text{-}T_{snow})/(T_{rain}\text{-}T_{snow}) & T_{snow} \le T_{mean} \le T_{rain} \\ 0 & T_{rain} \le T_{mean} \end{cases} \quad (2)$$

where Tsnow is the lower threshold temperature value (°C), and Train is the higher threshold temperature value (°C).

2.3.1.2. Snow accumulation

$$G = G + P \times S_p \quad (3)$$

$$eT_G = CTg \times eT_G + (1 - CTg) \times T_{mean} \quad (4)$$

where G is the snow accumulation (mm); CTg is the thermal state factor for snow cover; P is precipitation (mm) and eT_G is the thermal state of the snowpack (°C).

Table 1
Differences in methods and climate input in six versions of the Cemaneige module.

Version of Cemaneige	Rain/snow deviation	Snowmelt computation	Input variables[a]
M1	Double threshold function	Temperature exponential function	T,P
M2	Double threshold function	Seasonal snow melting factor	T,P
M3	Double threshold function	Temperature & radiation function	T,P,R
M4	Single threshold function	Temperature exponential function	T,P
M5	Single threshold function	Seasonal snow melting factor	T,P
M6	Single threshold function	Temperature & radiation function	T,P,R

[a] T – temperature, P – Precipitation and R – net Radiation

2.3.1.3. Snowmelt computation methods. Three snowmelt computation methods, temperature exponential function (Valéry et al., 2014b), seasonal snow melting factor (Wang and Melesse, 2005), and temperature & radiation function, were employed for snowmelt computation.

a) Temperature exponential function

$$\mathrm{PSNOWMELT} = \theta_{G1} \times \mathrm{T_{mean}} \quad \text{if} \quad \mathrm{eT_G} = 0 \quad \text{and } \mathrm{T_{mean}} > 0$$

$$\mathrm{SNOWMELT} = 0 \quad \text{otherwise} \tag{5}$$

where *PSNOWMELT* is the potential snowmelt ($mm \cdot d^{-1}$).

b) Seasonal snow melting factor

$$\theta_{G1} = \frac{\mathrm{SMFMX} + \mathrm{SMFMN}}{2} + \frac{\mathrm{SMFMX\text{-}SMFMN}}{2} \times sin\left[\frac{2\Pi}{365}(\mathrm{doy\text{-}106})\right] \tag{6}$$

$$\mathrm{PSNOWMELT} = \theta_{G1} \times \mathrm{T_{mean}} \quad \text{if} \quad \mathrm{eT_G} = 0 \quad \text{and } \mathrm{T_{mean}} > 0$$

$$\mathrm{PSNOWMELT} = 0 \quad \textit{otherwise} \tag{7}$$

where *SMFMX* represents the maximum snow melting factors ($mm \cdot d^{-1} \cdot ℃^{-1}$) on July 16; *SMFMN* represents the minimum snow melting factors ($mm \cdot d^{-1} \cdot ℃^{-1}$) on January 15 and *doy* is the ordinal number of days in a year.

c) Temperature & radiation function

$$\mathrm{PSNOWMELT} = \theta_{G1} \times \mathrm{T_{mean}} + \mathrm{RF} \times \mathrm{NetRad} \quad \text{if} \quad \mathrm{eT_G} = 0 \quad \text{and } \mathrm{T_{mean}} > 0$$

$$\mathrm{PSNOWMELT} = 0 \quad \textit{otherwise} \tag{8}$$

where *RF* is the radiation factor ($m^2 \cdot W^{-1} \cdot d^{-1} \cdot ℃^{-1}$) and *NetRad* represent the net radiation($W \cdot m^{-2}$).

2.3.1.4. Snow-cover accumulation

$$\textit{Snow covered area} = \frac{G}{G_{threshold}} \quad \textit{if} \quad G < G_{threshold}$$

$$\textit{Snow covered area} = 1 \quad \textit{otherwise} \tag{9}$$

where *Snow covered area* is the percentage of the snow cover and $G_{threshold}$ is the maximum of the snow accumulation.

More details (e.g., actual snowmelt computation and snowpack updating) of CemaNeige snowmelt modules can be referred to Valéry et al. (2014a, b). In this study, we only focus on the description of six versions of the Cemaneigh modules.

2.3.2. Potential evapotranspiration method

The potential evapotranspiration was estimated using the Oudin formulas based on extraterrestrial radiation (Oudin et al., 2005). The Oudin formula is expressed as

$$\mathrm{ETP} = \frac{R_e \times (T_{mean} + 5)}{\lambda \times \rho \times 100} \quad \textit{if} \quad T_{mean} + 5 > 0$$

$$ETP = 0 \quad \textit{otherwise} \tag{10}$$

where ETP is the potential evapotranspiration ($mm \cdot d^{-1}$), R_e is the extraterrestrial radiation ($MJ \cdot m^{-2}$) calculated in detail by Morton (1983), λ is the latent heat flux ($MJ \cdot m^{-2}$), and ρ is the water density ($kg \cdot m^{-3}$).

2.3.3. Hydrological model

The modèle du Génie Ruralà 4 paramètres Journalier (GR4J) is a daily-scaled, lumped, conceptual rainfall-runoff model with four parameters (Perrin et al., 2003). In this study, it has been amended to a semi-distributed model to cooperate with the snowmelt model. The GR4J model employs a production store and a routing store to calculate the daily streamflow generated by precipitation. Model input requires precipitation data and temperature data. The GR4J model cooperates with the Cemaneige model and performs pretty well in the daily streamflow simulation over many watersheds (Poissant et al., 2017; Troin et al., 2015; Velázquez et al., 2015; Zeng et al., 2019). Several hydrological model parameters are listed in Table 2, including GR4J and six versions of Cemaneige parameters.

2.4. Model calibration

The Shuffled Complex Evolution (SCE-UA) algorithm was applied to constrain the model parameters (Duan et al., 1994; Duan, 2021). The SCE-UA algorithm has been widely used in hydrological modeling for global optimization of parameters, and it has

integrated deterministic search strategies and random element sampling approaches (Rahnamay Naeini et al., 2019). We carried out a 10,000 multi-run and set the runoff as the single objective variable in our application. The simulation with the highest King-Gupta Efficiency (KGE) value in the multi-runs was used to identify the optimal parameterization in each model. We have put 2005–2008 as the calibration period and 2009–2011 as the validation period. The performance of each optimized model in simulating runoff for 2005–2008 is shown in Fig. S1.

To validate the model, we selected three metrics to evaluate the performance of the six optimized models identified in the model calibration. These metrics include KGE, Percentage Bias (PBIAS), Nash-Sutcliff Efficiency (NSE). The KGE metric with statistical nature comprehensively measure model performance from three aspects (i.e., correlation, variability bias, and mean bias). The correlation component represents the hydrological aspects of the model, such as peak flow times. The closer KGE is to 1, the better the model performance is obtained (Gupta et al.,2009; Knoben et al.,2019). PBIAS measures the average of simulated sequences (Moriasi et al., 2007). PBIAS= 0 indicates no bias, and the value below/above 0 ℃ indicates an underestimation/overestimation of the model. NSE matric reflects the similarity between observed and simulated runoff (Nash and Sutcliffe, 1970). NSE= 0 indicates the simulation corresponds to the observed mean runoff, and NSE= 1 indicates the simulated runoff has perfect performance.

The formulas for the calculation of KGE, PBIAS, and NSE are listed as follows:

$$KGE = 1 - \sqrt{\left(r\left(Q^{obs}, Q^{sim}\right) - 1\right)^2 + \left(\frac{\mu\left(Q^{obs}\right)}{\mu\left(Q^{sim}\right)} - 1\right)^2 + \left(\frac{\sigma\left(Q^{obs}\right)}{\sigma\left(Q^{sim}\right)} - 1\right)^2} \tag{11}$$

$$PBIAS = \frac{\sum_{t=1}^{T} Q_t^{sim}}{\sum_{t=1}^{T} Q_t^{obs}} - 1 \tag{12}$$

$$NSE = 1 - \frac{\sum_{t=1}^{T}\left(Q_t^{obs} - Q_t^{sim}\right)^2}{\sum_{t=1}^{T}\left(Q_t^{obs} - Q_{avg}^{obs}\right)^2} \tag{13}$$

In Eq. (11), Q^{obs} and Q^{sim} are the observed and simulated runoff series, $r\left(Q^{obs}, Q^{sim}\right)$ is the Person correlation coefficient between the observed and simulated runoff series, $\mu\left(Q^{obs}\right)$ and $\mu\left(Q^{sim}\right)$ are the average of the observed and simulated runoff series, $\sigma\left(Q^{obs}\right)$ and $\sigma\left(Q^{sim}\right)$ are the standard deviation of the observed and simulated runoff series; In Eqs. (12) and (13), Q_t^{sim} and Q_t^{obs} are the observed and simulated runoff at time t, T is the number of runoff samples.

2.5. climate bias-correction

To make historical baseline conditions of GCM data be in line with the observation data sets, a linear-scaling approach with multiplication and addition (Lenderink et al., 2007) was applied to precipitation and temperature, respectively, for their time series of 1961–2005. The linear-scaling approach is formulated as follows:

$$P_t^{adj} = P_t^{ori} \times \frac{P_{avg}^{obs}}{P_{avg}^{ori}} \tag{14}$$

$$T_t^{adj} = T_t^{ori} + \left(T_{avg}^{obs} - T_{avg}^{ori}\right) \tag{15}$$

where P_t^{adj} and P_t^{ori} are the adjusted and original precipitation series of GCM data, T_t^{adj} and T_t^{ori} are the adjusted and original temperature series of GCM data.

To evaluate how well the GCM dataset have been bias-corrected, another three indices (i.e., coefficient of determination (R^2), root mean square deviation (RMSD), and bias) were calculated based on the individual GCM dataset or mean of the multi-model ensemble (MME) and the CN05.1 data for the historical period (1961–2005). R^2 reflects the fitting degree between the GCM dataset and

Table 2
Description of model parameters in the hydrological model.

Parameters	Description	Unit	Sampling range	
			Lower bound	Upper bound
x_1	The capacity of production storage	mm	1	750
x_2	Groundwater exchange coefficient	mm/d	-10	10
x_3	The capacity of routing storage	mm	1	400
x_4	Routing time of unit hydrograph	Days	0.5	10
θ_{G1}	Degree factor for snowmelt	$mm{\cdot}d^{-1}{\cdot}^{\circ}C^{-1}$	0	10
CTg	Thermal state factor for snow cover	non-dimensional	0	1
SMFMX	Maximum snow melting factors	$mm{\cdot}d^{-1}{\cdot}^{\circ}C^{-1}$	0	10
SMFMN	Minimum snow melting factors	$mm{\cdot}d^{-1}{\cdot}^{\circ}C^{-1}$	0	10
RF	Radiation factor	$m^2{\cdot}mm{\cdot}W^{-1}{\cdot}d^{-1}{\cdot}^{\circ}C^{-1}$	0	1

observations; RMSD quantifies the dispersion between the GCM dataset and observations; Bias reflects the GCM dataset overestimation and underestimation relative to observations. These indices are formulated as follows:

$$R^2 = 1 - \frac{\sqrt{\sum_{i=1}^{n}(M_i - O_i)^2}}{\sqrt{\sum_{i=1}^{n}(O_i - O_{avg})^2}} \tag{16}$$

$$RMSD = \left[\frac{1}{n}\sum_{i=1}^{n}(M_i - O_i)^2\right]^{\frac{1}{2}} \tag{17}$$

$$Bias = M_{avg} - O_{avg} \tag{18}$$

In Eqs. (16) - (18), M_i and O_i are the GCM dataset and observation respectively , M_{avg} and O_{avg} are the average of the GCM dataset and observation, respectively, and n is the number of samples.

2.6. Center of mass date for snowmelt

The center of mass date (CMD) was used to estimate the impact of climate change on the timing of snowmelt when 50% of the total annual snowmelt occurred. This method was used in previous studies to calculate the time center of snowmelt runoff. The annual snowmelt centers are calculated as follows:

$$CMD = \frac{\sum_{i=1}^{T}(SM_i t_i)}{\sum_{i=1}^{T} t_i} \tag{19}$$

where t_i represents the number of days in a year and SM_i represents the snowmelt on the corresponding date.

2.7. Relative importance of dominant factors

To identify the dominant factors that regulate the inter-annual variations of runoff in the future plausible climate change scenarios, we used a random forest algorithm from the Statistics and Machine Learning Toolbox of Matlab (Loh, 2002) to assess the relative importance of predictive factors that can explain the variance of runoff. This analysis selected temperature, precipitation, evapotranspiration, snowmelt, and snowmelt timing as the predictive factors. The daily streamflow was the response factor. The tree-based methods construct hierarchical binary decision trees, which can avoid model over-fitting. Predictor importance is estimated by computing the out-of-bag accuracy before and after permutation, and the accuracy differences mean the influence of a predictor variable on the response variable (Nicodemus et al., 2010). The average of accuracy changes of all trees represents the final importance scores—the importance of the variable increases with the value of this measure. The split predictor at each node is specified using an interaction-curvature test to grow unbiased trees, and the total dataset was used to train a regression tree. The workflows of the entire study are illustrated in the schematic diagram (Fig. 2).

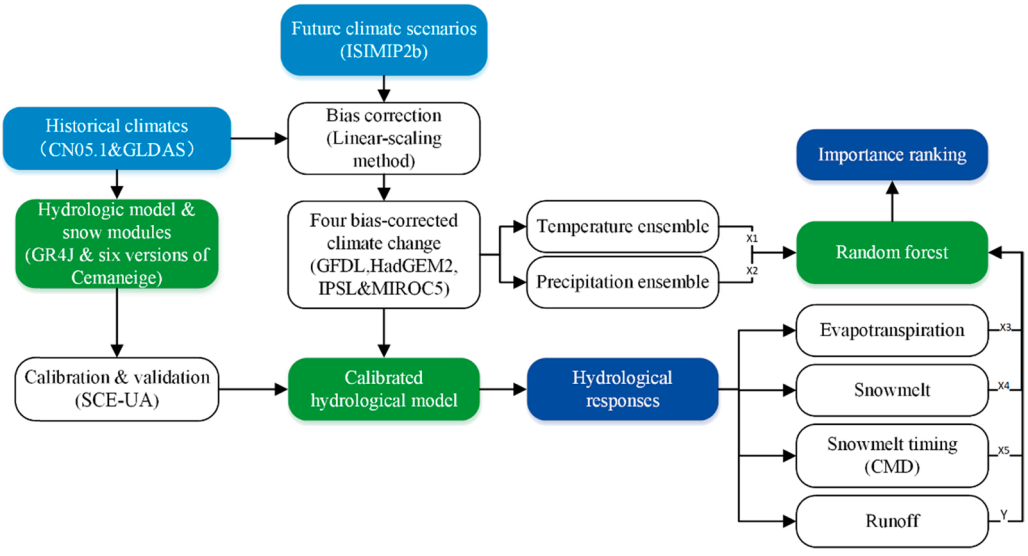

Fig. 2. A diagram to illustrate the analysis workflow for this study.

3. Results

3.1. Validation of daily runoff simulation

The performances of the hydrological model with six different snowmelt modules in simulating runoff were validated based on three indices (i.e., KGE, PBIAS, and NSE) during the period (2009–2011) (Fig. 3). For KGE values, all six models showed reasonable simulations with the values of KGE ranging from 0.62 to 0.73. However, both M1 (the version with single threshold function and temperature exponential function, as shown in Table 1) and M5 (the version with Double threshold function and Seasonal variation degree factor, as shown in Table 1) showed relatively lower PBIAS values: 2.64% (M1) and 4.96% (M5). Besides, M5 also had the highest NSE value (NSE=0.58) and thus was selected to project runoff in the future.

The seasonal variations of daily runoff for the model simulations and observations during 2009–2011 were illustrated (Fig. 4). The calibrated models can generally capture seasonal variations of the runoff, particularly for the hydrological responses to summer and autumn rainfall. However, the models also showed larger deviations from the observed runoff during the early snowmelt period. The snowmelt period in the Kaidu River Basin often starts from April to May. As temperature rises, snowmelt runoff increases, and spring floods may occur. The discrepancy between simulations and observations was more evident in 2010 and 2011, during which the larger snowmelt-induced peaks were observed than that in previous years. For the timing of spring flood arrivals, the model with either the STT or DTT method can efficiently simulate it. However, when it comes to the larger spring floods, like 2010 and 2011, all the snowmelt models showed less efficiency in capturing the magnitude of floods than their performance in the calibration period (Fig. S1 and Fig. 4).

Among the six models, the M5 snowmelt model simulated a relatively better variation of spring runoff than other models in 2010. However, it also overestimated the magnitude of the first runoff peak as many other models. As the M5 snowmelt model used a degree-day factor accounting for the day number of the year, it can better represent the effects of seasonal variations in the solar radiation on snowmelt. The albedo of the snow also has a seasonal variation because fresh snow is commonly found in the mid-winter, and aged snow is found in the late winter and spring.

The possible reasons to explain the model's inefficiency in capturing the magnitude of spring runoff peaks can be (1) the reliabilities of snowfall measurements; (2) large variabilities of spring temperature, which may cause several rapid snow melting or refreezing events; (3) the spatial effects (for instance, the topography of catchment and alpine snow distribution) on the catchment snowmelt during the occurrence of larger spring floods, which can be a major challenge for these temperature index-based models to simulate the magnitude of spring floods.

3.2. Bias-correction evaluation for precipitation and temperature

Before running scenario simulations with the optimal hydrological model, four GCMs data were bias-corrected based on the observational data set. Three indices were used to assess the bias-corrected precipitation and temperature in each GCM dataset and MME against the CN05.1 dataset for the historical period (1961–2005) (Table 3). The mean bias between simulated precipitation and temperature and observed data was basically eliminated through the linear-scaling approach. It is evident that the bias correction improved both R^2 and RMSD. After correction, the R^2 and RMSE value of MME is 0.60, 0.56 for precipitation while 0.94, 3.27 for temperature, respectively. Moreover, MME showed better performance than individual GCM in Table 3, with the results of the

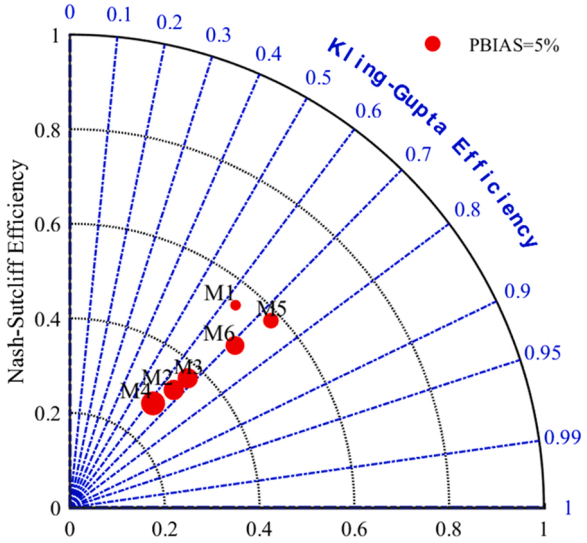

Fig. 3. Parameter results of six versions during validation. The angle represents KGE, and radius represents NSE; marker size reflects PBIAS.

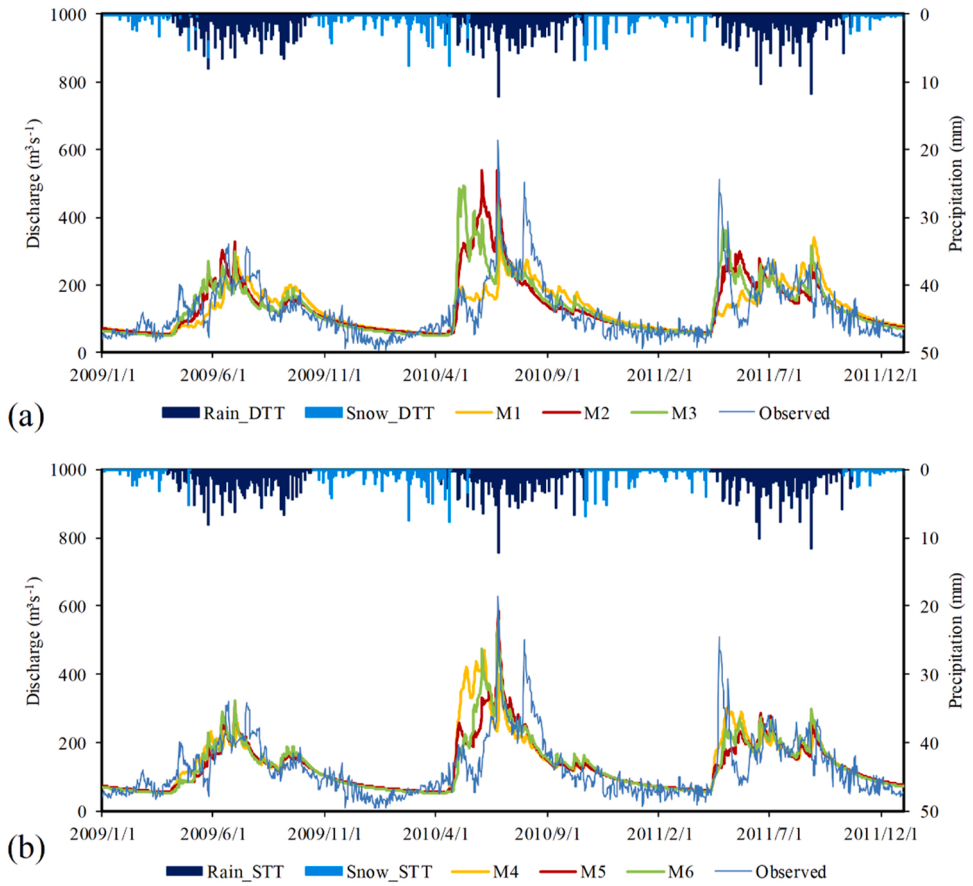

Fig. 4. Runoff simulated by the hydrological model with six versions of snowmelt modules (M1-M6) for the Kaidu River Basin during the calibration period (2009–2011). The two sub-graphs represent different solid-liquid separations: (a) double threshold and (b) single threshold. Rain_STT and Snow_STT represent the rain and snow calculated by STT. Rain_DTT and Snow_DTT represent the rain and snow calculated by DTT.

correction analysis shown in Fig. S2.

The inter-annual variations also indicated that the adjusted data of four GCMs could capture the magnitude and variabilities of precipitation and temperature in the study area. In contrast, MME had better performance than the individual model during the historical period (1961–2005) (Fig. 5).

3.3. *Snowmelt-driven Runoff under climate change*

The results of hydrological simulation under three different RCPs (RCP2.6, RCP4.5, and RCP8.5) with input data from four GCMs were studied in order to explore the variations of runoff in the future periods. We mainly focused on the results based on the ensemble mean of simulations. The changes in future runoff were analyzed during mid-century (2036–2065) and the end-century (2070–2099)

Table 3
Statistics of precipitation and temperature in four GCMs during the historical period (1961–2005).

		R^2		RMSD (mm/℃)		Bias (mm/℃)	
		original	adjusted	original	adjusted	original	adjusted
Precipitation	GFDL	-0.54	-2.56	1.10	1.67	-0.64	0.00
	HadGEM2	0.59	0.64	0.57	0.53	-0.39	0.00
	IPSL	0.23	-0.19	0.77	0.96	-0.40	0.00
	MIROC5	0.48	0.46	0.64	0.65	-0.42	0.00
	MME	0.46	0.60	0.65	0.56	-0.40	0.00
Temperature	GFDL	0.89	0.93	4.44	3.55	-2.66	0.00
	HadGEM2	0.89	0.93	4.45	3.54	2.69	0.00
	IPSL	0.88	0.92	4.57	3.78	2.58	0.00
	MIROC5	0.89	0.93	4.30	3.41	2.61	0.00
	MME	0.90	0.94	4.20	3.27	2.63	0.00

relative to the baseline period (1976–2005) under RCP2.6, RCP4.5, and RCP8.5 (Fig. 6). For mid-century, there was little difference in the proportion of runoff reduction among the three RCPs. Compared with the reference period, decreases in the mean annual runoff for the mid-century period were 12.81% (−25.44 $m^3 \cdot s^{-1}$), 17.19% (−34.14 $m^3 \cdot s^{-1}$), and 13.50% (−26.83 $m^3 \cdot s^{-1}$) under three RCPs, respectively. However, for the end-century, the runoff of RCP8.5 had declined by about two times than that in mid-century, while the runoff of RCP4.5 fluctuated steadily and the runoff of RCP2.6 recovered basically to the level of the baseline period. The runoff simulation under RCP 2.6, RCP4.5, and RCP8.5 showed decreases of 3.38% (−6.72 $m^3 \cdot s^{-1}$), 15.82% (−31.41 $m^3 \cdot s^{-1}$), and 24.26% (−48.21 $m^3 \cdot s^{-1}$) as compared with the reference period as shown in Fig. 6. The simulated annual and seasonal (except spring) runoff showed declining trends ($p < 0.05$) under RCP4.5 and RCP8.5 (Table 4). On the other hand, the simulated evapotranspiration showed a significant increasing trend ($p < 0.05$) under different RCPs. At the same time, the precipitation and runoff illustrate an insignificant trend in RCP2.6 and RCP4.5, which was similar to a previous study (Li et al., 2019). The increase of water vapor in the atmosphere did not produce sufficient precipitation due to temperature rising in the study area, precipitation, and temperature-induced the decrease of runoff together.

Besides the change of annual runoff, the variations of seasonal runoff during the whole period were projected and evaluated, as shown in Fig. 6. The projection of runoff values shows large variations in seasons. The runoff in summer under three RCPs shows the largest decrease among the four seasons (the details of the trends are shown in Table 4), followed by autumn and winter, while that in spring rises slowly. At the same time, the summer runoff decrease is similar to the annual runoff under three PCRs. During mid-century, the proportion of summer runoff in RCP 2.6, 4.5 and 8.5 decreased by 15.74% (−64.32 m^3/s), 18.87% (−77.10 m^3/s) and 15.33% (−62.69 m^3/s) compared with that in the baseline period, while decrease by 3.20% (−13.08 m^3/s), 19.74% (−80.67 m^3/s) and 29.70% (−121.46 m^3/s) during end-century (as shown in Fig. 6).

The largest variabilities were found in summer for inter-annual variabilities of annual and seasonal runoff during three periods (historical, mid-century, and end-century) from three RCPs (Fig. 7). In summer, compared to the historical period, both RCP2.6 and RCP 4.5 showed a decline in mid-century and a rise in end-century for the seasonal mean runoff; however, RCP8.5 showed a continuous decline from mid-to end-century. For the range of variabilities, both RCP2.6 and RCP4.5 predicted an increase from mid-to end-century, suggesting that the year-to-year fluctuation of summer runoff was enhanced as the climate warms; nevertheless, RCP8.5 showed an opposite tendency of change. The spring runoff showed a general increase with time in three RCPs, especially in RCP8.5, indicating the future climate impact on snowmelt. Meanwhile, the inter-annual variabilities of evapotranspiration did not show a large shift for the range and magnitude among three RCPs, whereas the variability of precipitation decreases sharply in the larger future warming scenario (Fig. S3). Therefore, precipitation is inferred to be the principal factor that causes changes in the runoff variability.

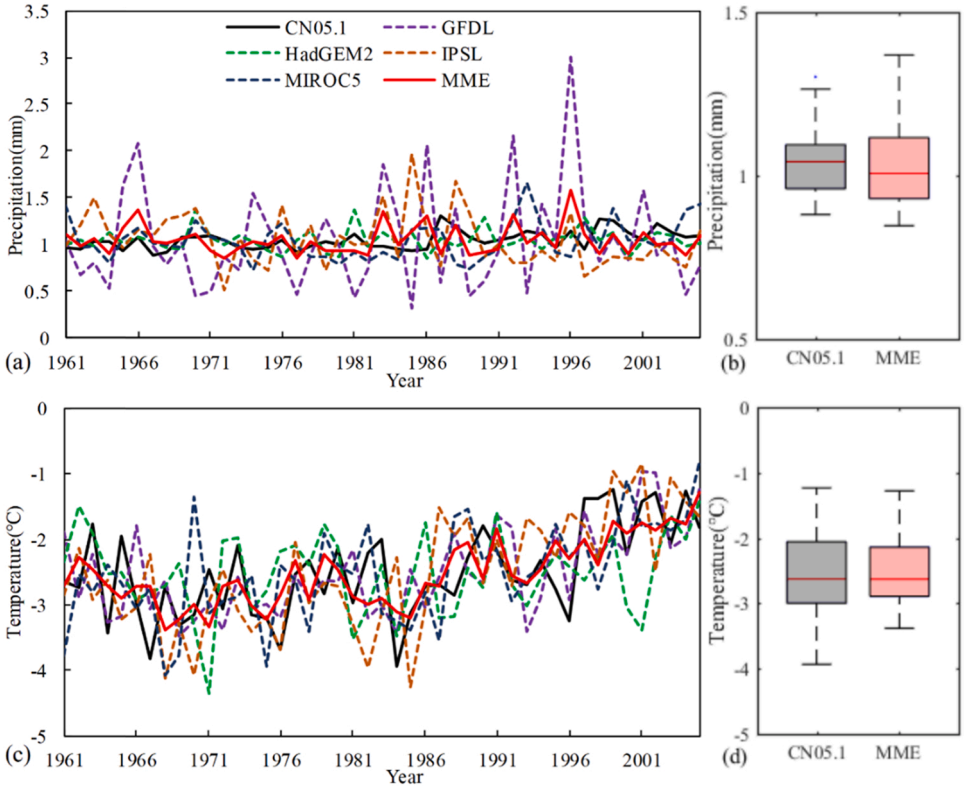

Fig. 5. Inter-annual variations (a, c) and periodical variabilities (b, d) of temperature and precipitation for CN05.1 and ISIMIP2b climate data sets during the historical period (1961–2005). The boxes represent the 25th and 75th percentiles, red lines represent the 50th percentiles, and whiskers represent the maximum and minimum except outliers.

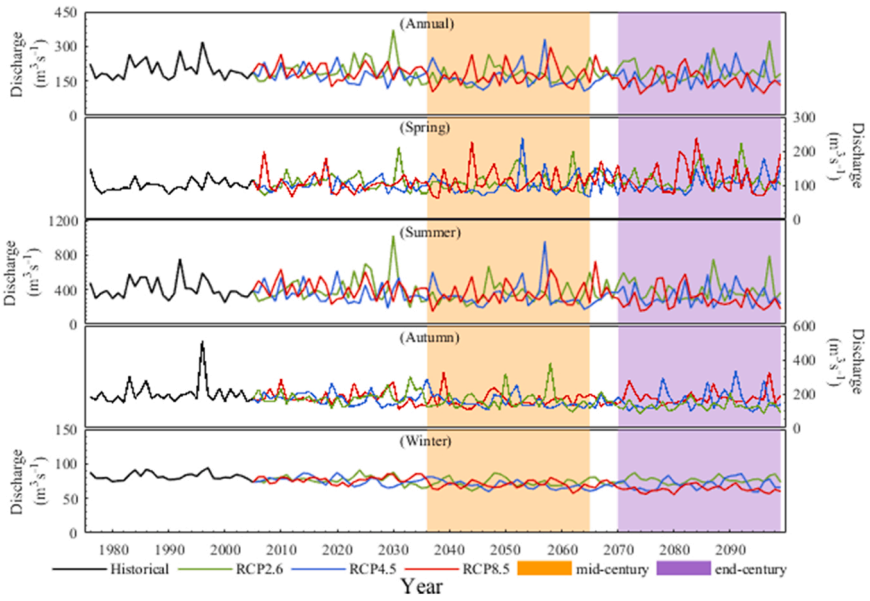

Fig. 6. Inter-annual variations of annual and seasonal (March-May for spring, June-August for summer, September-November for autumn, and December-February for winter) runoff under RCP2.6, RCP4.5, and RCP8.5 from 1976 to 2099. The results showed the ensemble mean of four GCM driven runs. Mid-century represents (2036–2065) and the end-century represents (2070–2099).

Table 4
Trends in the average of multiple patterns under three RCPs. The trends of precipitation are based on the bias-corrected data sets from ISIMIP2b.

		Annual	Spring	Summer	Autumn	Winter
Runoff(10^{-3} mm·d^{-1})	RCP2.6	0.096	0.644	-0.050	-0.178	-0.037
	RCP4.5	-0.785	0.615	-2.522	-0.826	**-0.398**
	RCP8.5	**-2.513**	0.976	**-7.356**	**-2.848**	**-0.797**
Precipitation(10^{-3} mm·d^{-1})	RCP2.6	0.435	1.206	0.539	0.118	-0.138
	RCP4.5	0.212	**1.931**	-1.892	0.542	0.270
	RCP8.5	-0.753	**2.606**	**-6.272**	-0.343	**1.032**
Evapotranspiration (10^{-3} mm·d^{-1})	RCP2.6	**0.551**	**0.897**	**0.781**	**0.511**	0.001
	RCP4.5	**2.175**	**2.387**	**4.373**	**1.889**	**0.006**
	RCP8.5	**5.051**	**5.769**	**9.787**	**4.487**	**0.057**

Note: The values with the bold type indicate that the trend is statistically significant ($P < 0.05$).

4. Discussions

4.1. Runoff responses to climate change

This study studies the future change of runoff for the Kaidu River Basin under plausible future warming scenarios and provides new insights on understanding the hydrological responses to climate change. The causes of runoff changes are largely associated with different hydrological processes under climate change. Evapotranspiration is a vital hydrological process for the water cycle (Yang et al., 2021). Previous studies show that there is inconformity between the simulated runoff and evapotranspiration. Based on the simulations using the SWAT model forced by RCMS/GCMS under different concentration scenarios, some researchers concluded that the main factor leading to decreased runoff in the future is increased evapotranspiration (Ba et al., 2018; Fang et al., 2018). However, we also observed that future precipitation and temperature trends might differ between GCMs in this study area. As the precipitation varies largely among different climate models and these differences may affect the accuracy of runoff simulation in this area (Zhang et al., 2006; Tian et al., 2017), precipitation may introduce large uncertainty in the projection of runoff and complicate the understanding of underlying drivers of hydrological responses of runoff. Previous studies also showed the reliability of the gridded climate dataset applied for this study area (Luo et al., 2020). Similar to those studies, to bias-correct the ISIMIP2b climate trajectories based on the best available historical observation data (i.e. CN05.1) can improve the robustness of our predictions of future climate change impacts on regional hydrological processes.

The model structure and snowmelt modules are also important factors to cause uncertainties of the runoff projection (Najafi et al., 2011; Feng & Beighley, 2020). In the snowmelt model, the temperature index method often depends on the mean air temperature. However, Zhang et al. (2006) found that using the daily maximum temperature multiplied by 0.5 as one of the model inputs improved

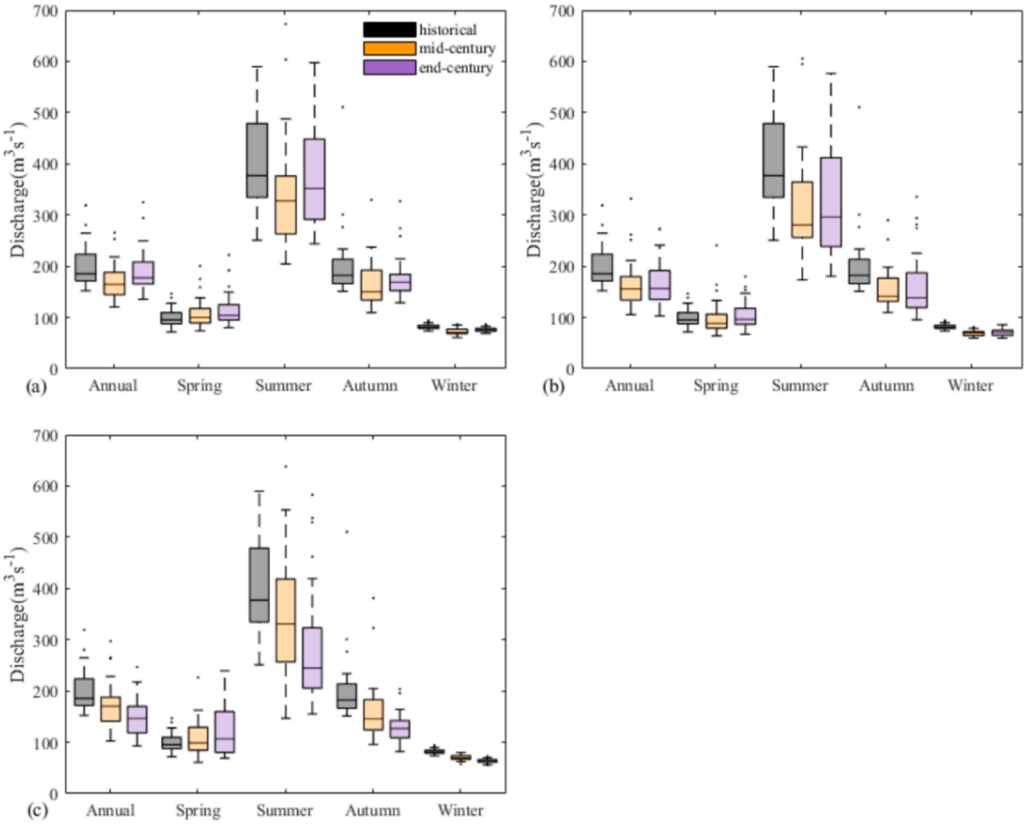

Fig. 7. The inter-annual variabilities of annual and seasonal runoff for historical, mid-and end-century under (a) RCP2.6, (b) RCP4.5, and (c) RCP8.5 scenarios. The boxes represent the 25th and 75th percentiles, the middle lines represent the 50th percentiles, and whiskers represent the maximum and minimum.

snow cover mapping than the simulations with daily mean temperature as the model input. Therefore, the temperature index method could consider the daily maximum air temperature as one of the climatic inputs to estimate snowmelt. Thus, the optimization of the hydrological model offers fairness in the model choice. Using the maximized KGE values as an optimized object in the calibration stage, we evaluated the models' performances by NSE and PBIAS values. We studied the effects of climate change under the assumption that the best set of parameters found during the calibration process in historical periods will remain valid in the future.

The responses of runoff on climate change can imply a potential water shortage in the future. To quantify the trends of runoff, we adopted a 30-year moving average to smooth the runoff fluctuations and detect how the change in the trends of runoff is in response to climate warming (Fig. 8). In general, the annual runoff showed different tendencies of changes in the three RCPs. The inter-annual patterns of these changes were mostly dependent on summer-time runoff. We found the trends with a strong fluctuation in RCP2.6, a slow increase in RCP4.5, and both of them end with a small positive trend. However, RCP8.5 runoff trends went up generally before 2057 but then dropped rapidly to $-0.79\ m^3s^{-1}a^{-1}$ in 2099. Meanwhile, the runoff trend in autumn was consistent with each other among three RCPs before 2050, while that of RCP2.6 and RCP4.5 both turned positive and reach $0.39\ m^3s^{-1}a^{-1}$ and $0.69\ m^3s^{-1}a^{-1}$ respectively in 2099, similar to that in winter, which reached $0.10\ m^3s^{-1}a^{-1}$ and $0.12\ m^3s^{-1}a^{-1}$ respectively. The spring runoff trend distinguished obviously from the other three seasons, and it showed lasting positive under RCP8.5, whereas dramatic fluctuation under RCP2.6 and RCP4.5, by the time, almost disappeared at the end of the 21st century. The absolute value of the trend under RCP8.5 was larger than that under other scenarios for both annual and seasonal runoff.

4.2. *Timing of snowmelt*

Another issue related to the snowmelt runoff simulation is the timing of the snowmelt. Compared to studies in other countries, like the United States, Canada, Japan, etc., the timing of snowmelt in China is less studied (McCabe and Clark, 2004; Dyer, 2008). We used snowmelt CMD to describe the variations in the snowmelt's timing and fitted the CMD trends using the least square method. The general trend for CMD was a linear decline over the historical period but continued with different directions of polynomial trends under three RCPs, suggesting how early snowmelt advances depended on the level of future warming. The changes in snowmelt time was significantly different under different scenarios, and the fitting curve formula is shown in Fig. 9. Compared with the historical period (1976–2005), the CMD decline trend of the three RCP scenarios before the mid-century was similar to that of the historical

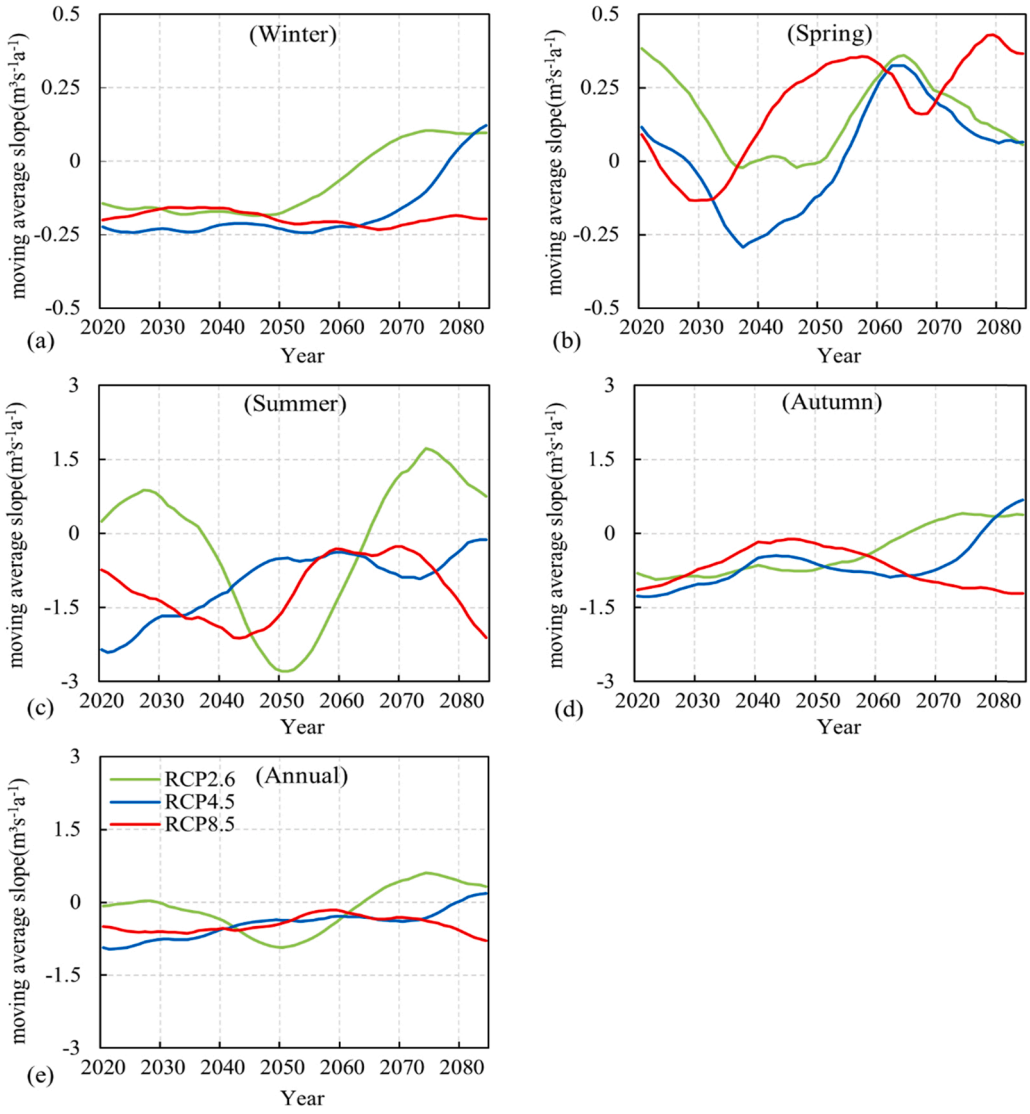

Fig. 8. Changes in the trend based on 30-year moving-average of annual runoff in three decades.

period. However, after the mid-century, the RCP8.5 CMD continued the trend in the historical period, and the RCP4.5 CMD slowed down significantly while the trend of CMD under RCP2.6 showed the snowmelt time started to recover gradually after 2055. Compared with the historical period (1976–2005), the timing of snowmelt under three warming scenarios at the end of this century (2070–2099) was 8.2, 13.9, and 25.5 days earlier, respectively. This suggests that the effects of different anthropogenic warming scenarios on snowmelt CMD have similar effects in the short-term and distinct effects in the long term.

4.3. Relative importance of climate-related drivers on future runoff

The relative importance of predictive factors (i.e., precipitation, temperature, evapotranspiration, snowmelt timing and, snowmelt) to the response variable (runoff) was explored based on a random forest model and the historical and three RCP simulation data sets (Fig. 10 and Fig. S4). To better compare the relative importance of drivers in different scenario runs, we rescale the importance of individual drivers by dividing it with the total importance, the sum of the importance of all individual factors. Precipitation was the predominant factor for the spring-to-autumn runoff, and evapotranspiration was the second important factor in all three RCP scenarios (Fig. 10). However, during the historical period, snowmelt timing was the second important factor. The importance of snowmelt timing declined in the warmer RCP scenarios, indicating that earlier advance of snowmelt may reduce its contribution to the total runoff from spring to autumn.

On the contrary, the importance of temperature and precipitation increased in a warmer RCP scenario. However, for the spring runoff, snowmelt is the second important factor in the historical and RCP2.6 scenario (Fig. S4). The effects of evapotranspiration in

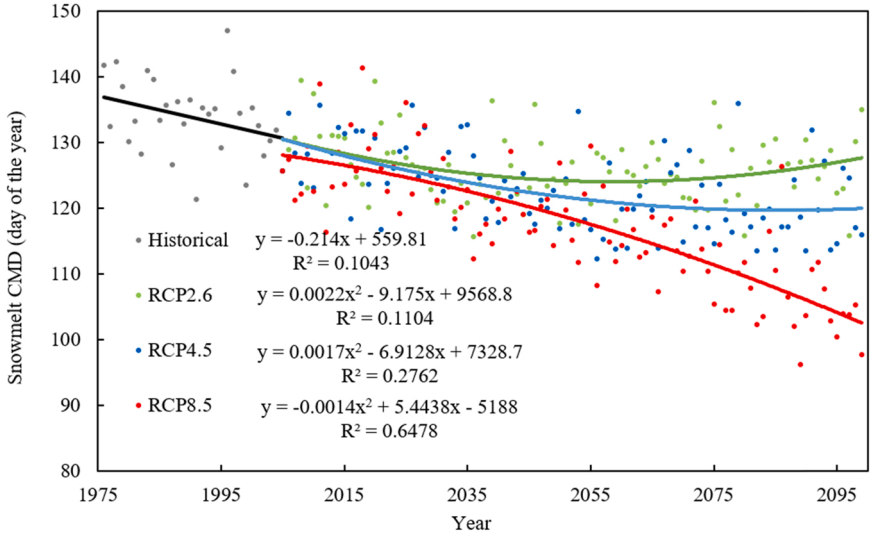

Fig. 9. A scatter diagram of snowmelt center of mass date (CMD) under historical and RCP periods (1976–2099).

spring runoff are less important than its effects on summer and autumn runoff. In the meantime, with the increase of concentration scenarios, the importance of snowmelt timing strengthens relatively, but snowmelt reduces its importance, while temperature importance basically was equivalent to evapotranspiration importance in the higher RCP scenarios.

Our results partly agree with the conclusion of previous studies, for instance, Chen et al. (2014, 2015), which suggest that precipitation and temperature are the main factors regulating the runoff variations in the Kaidu River Basin. Unlike other alpine river basins (e.g., the Kunmalik and Hotan River Basins), the major influential factor of the runoff variation is the temperature (Shen et al., 2018; Luo et al.,2017). Chen et al. (2017) has highlighted the importance of including glacier melt in the hydrological modeling of the glacierized catchments, which can be a critical perspective that should be accounted for in the study of hydrological responses to future climate change. Higher climatic warming may enhance glacier melt and increase the contribution of headwater to streamflow, compensating for the negative response of runoff to warming. We speculate that if our model considers the effects of the glacier- or ice melt, they will become more important factors to determine runoff, similar to what our historical simulation has indicated.

4.4. Future study

Although the regional coverage of the Kaidu River Basin is mostly in mountainous areas, vegetation types can still be an important factor to affect the change of runoff. Some studies (e.g., Mamat et al., 2021; Wang et al., 2021) have shown that the response of vegetation to climate change may substantially impact the soil moisture in the ecosystem and total evapotranspiration. Moreover, human activities can be another important factor to be considered in the projection of future runoff. Chen et al. (2013) found that during 1994–2009, despite that runoff in Kaidu River Basin is more sensitive to climate variability than human activities, which had already contributed 9.5% of the increase in runoff. Therefore, accounting for future changes in the potential natural vegetation distribution, land use and land cover change, human activities, topographical features associated with snow distribution, and glacier melt, the importance of dominant climatic drivers of runoff in the Kaidu River Basin can be more explicitly represented.

5. Conclusions

This study evaluated the simulations of outlet-observed runoff under the observed gridded climate data sets based on a hydrological model with six versions of the Cemaneige snowmelt module. First, after bias-correction of future climate data sets, how runoff was in response to climate change under three RCP scenarios was quantified. Then, the 30-year moving average runoff was used to analyze the trend change every 30 years, and the CMD was used to indicate the timing of the snowmelt. Finally, we analyzed the importance of variables that determine the trend and variations of runoff in summer using the random forest algorithm.

Through KGE calibration and PBIAS and NSE evaluation, the M5 combined by single threshold function and seasonal snowmelt factor was more suitable for runoff simulation in the study area with three index values are 0.73, 4.96%, and 0.58, respectively. Therefore, the difference of simulation and observation sequence during the calibrated period was particularly manifest in the early stage of snowmelt.

Under the RCP scenarios, annual runoff responded to global warming trends with about a 15% reduction during the mid-century. For the end-century, RCP8.5 runoff declined by about two times that in mid-century, while RCP4.5 fluctuated steadily and RCP2.6 recovered basically to that in the baseline period, which is mainly determined by summer runoff. Meanwhile, the magnitude of the trend under RCP8.5 is more significant than that of other RCPs for both annual and seasonal runoff. The timing of the snowmelt in the

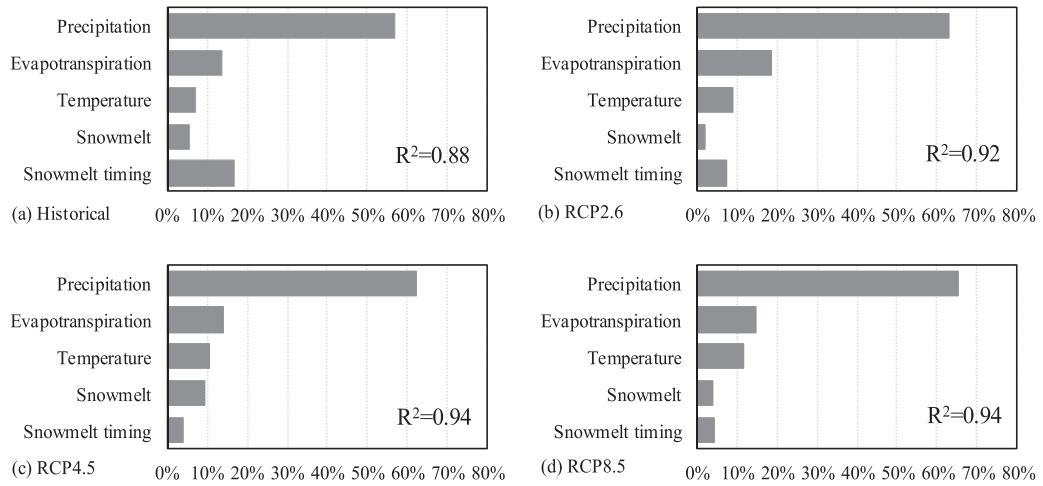

Fig. 10. Ranked importance of variables to explain runoff in spring-to-autumn runoff based on historical and three RCP simulations.

future showed a distinct pattern of temporal change in three RCPs, suggesting that the timing of the snowmelt was also associated with the extent of warming. Precipitation and evapotranspiration were the two most important factors contributing to future runoff from spring to autumn, which partly agrees with previous studies. But with the increase of warming, the timing of snowmelt turned to be less important, while the importance of precipitation increased relatively.

Overall, our results have revealed the potentially important drivers in controlling future trends of runoff in the Kaidu River Basin and also highlighted that the runoff prediction in this region should not only account for the processes related to snowmelt but also other factors, like glacier melt, land use, and land cover change and human activities, which will be included in our future hydrological modeling study.

CRediT authorship contribution statement

Bingqian Zhao: Methodology, Writing – original draft, Validation, Visualization. **Huaiwei Sun:** Conceptualization, Methodology, Writing, Supervision, Project administration. **Dong Yan:** Supervision. **Guanghui Wei**: Resources. **Ye Tuo**: Writing. **Wenxin Zhang:** Funding acquisition, Writing.

Declaration of Competing Interest

The authors declare that they have no known competing financial interests or personal relationships that could have appeared to influence the work reported in this paper.

Acknowledgments

The authors thank the financial support of the Ministry of Science and Technology (2019FY00205), the NSFC-STINT (52011530128), and NSFC (51879110, and 52079055). We also thank Prof. Jingfeng Wang at the Georgia Institute of Technology for his valuable comments on the methodology and thank Prof. Jianzhong Zhou and Lu Chen at Huazhong University of Science and Technology for their constructive suggestions on the manuscript preparation.

Appendix A. Supporting information

Supplementary data associated with this article can be found in the online version at doi:10.1016/j.ejrh.2021.100968.

References

Alfieri, L., Burek, P.A., Feyen, L., Forzieri, G., 2015. Global warming increases the frequency of river floods in Europe. Hydrol. Earth System Sci. 19 (5), 2247–2260 http://doi.org/doi.org/10.5194/hess-19-2247-2015.

Arsenault, R., Brissette, F., Martel, J., 2018. The hazards of split-sample validation in hydrological model calibration. J. Hydrol. 566, 346–362. https://doi.org/10.1016/j.jhydrol.2018.09.027.

Azmat, M., Qamar, M.U., Huggel, C., Hussain, E., 2018. Future climate and cryosphere impacts on the hydrology of a scarcely gauged catchment on the Jhelum river basin, Northern Pakistan. Sci. Total Environ. 639, 961–976. https://doi.org/10.1016/j.scitotenv.2018.05.206.

Ba, W., Du, P., Liu, T., Bao, A., Luo, M., Hassan, M., Qin, C., 2018. Simulating hydrological responses to climate change using dynamic and statistical downscaling methods: a case study in the Kaidu River Basin, Xinjiang, China. J. Arid Land 10 (6), 905–920. https://doi.org/10.1007/s40333-018-0068-0.

Bao, A., Huang, Y., Ma, Y., Guo, H., Wang, Y., 2017. Assessing the effect of EWDP on vegetation restoration by remote sensing in the lower reaches of Tarim River. Ecol. Indic. 74, 261–275. https://doi.org/10.1016/j.ecolind.2016.11.007.

Chen, Z., Chen, Y., Li, B., 2013. Quantifying the effects of climate variability and human activities on runoff for Kaidu River Basin in arid region of northwest China. Theor. Appl. Climatol. 111, 537–545. https://doi.org/10.1007/s00704-012-0680-4.

Chen, Y., 2014. Water Resources Research in Northwest China. Springer, Dordrecht. https://doi.org/10.1007/978-94-017-8017-9.

Chen, Y., Li, Z., Fan, Y., Wang, H., Deng, H., 2015. Progress and prospects of climate change impacts on hydrology in the arid region of northwest China. Environ. Res. 139, 11–19.

Chen, Y., Li, W., Deng, H., Fang, G., Li, Z., 2016. Changes in Central Asia's water tower: past, present and future. Sci. Rep. 6, 35458. https://doi.org/10.1038/srep35458.

Chen, Y., Li, W., Fang, G., Li, Z., 2017. Hydrological modeling in glacierized catchments of Central Asia: 2 status and challenges. Hydrol. Earth System Sci. 21 (2), 669–684. https://doi.org/10.5194/hess-2016-325.

Coppola, E., Raffaele, F., Giorgi, F., 2018. Impact of climate change on snow melt driven runoff timing over the alpine region. Clim. Dyn. 51 (3), 1259–1273. https://doi.org/10.1007/s00382-016-3331-0.

Dahri, Z.H., Ludwig, F., Moors, E., Ahmad, S., Ahmad, B., Ahmad, S., Riaz, M., Kabat, P., 2021. Climate change and hydrological regime of the high-altitude Indus basin under extreme climate scenarios. Sci. Total Environ. 768, 144467 https://doi.org/10.1016/j.scitotenv.2020.144467.

Deng, H., Chen, Y., Wang, H., Zhang, S., 2015. Climate change with elevation and its potential impact on water resources in the Tianshan Mountains, Central Asia. Glob. Planet. Chang. 135, 28–37. https://doi.org/10.1016/j.gloplacha.2015.09.015.

Duan, Q. ,2021. Shuffled Complex Evolution (SCE-UA) Method. MATLAB Central File Exchange. Retried from https://www.mathworks.com/matlabcentral/fileexchange/7671-shuffled-complex-evolution-sce-ua-method.

Duan, Q., Sorooshian, S., Gupta, V.K., 1994. Optimal use of the SCE-UA global optimization method for calibrating watershed models. J. Hydrol. 158 (3), 265–284 http://doi.org/doi.org/10.1016/0022-1694(94)90057-4.

Dyer, J., 2008. Snow depth and streamflow relationships in large North American watersheds. J. Geophys. Res. Atmos. 113 (D18), D18113. https://doi.org/10.1029/2008JD010031.

Edijatno, Nascimento N.D., Yang, X.L., Makhlouf, Z., Michel, C., 1999. GR3J: a daily watershed model with three free parameters. Hydrol. Sci. J. 44 (2), 263–277.

Fang, G., Yang, J., Chen, Y., Li, Z., De Maeyer, P., 2018. Impact of GCM structure uncertainty on hydrological processes in an arid area of China. Hydrol. Res. 49 (3), 893–907. https://doi.org/10.2166/nh.2017.227.

Feng, D., Beighley, E., 2020. Identifying uncertainties in hydrologic fluxes and seasonality from hydrologic model components for climate change impact assessments. Hydrol. Earth System Sci. 24 (5), 2253–2267.

Fortin, V., Turcotte, R. , 2007. Le modèle hydrologique MOHYSE, Note de cours pour SCA7420. Report. Département des sciences de la terre et de l'atmosphere, Université du Québeca Montreal, Canada, 17pp.

Frieler, K., Lange, S., Piontek, F., Reyer, C.P.O., Schewe, J., Warszawski, L., Zhao, F., Chini, L., Denvil, S., Emanuel, K., Geiger, T., Halladay, K., Hurtt, G., Mengel, M., Murakami, D., Ostberg, S., Popp, A., Riva, R., Stevanovic, M., Suzuki, T., Volkholz, J., Burke, E., Ciais, P., Ebi, K., Eddy, T.D., Elliott, J., Galbraith, E., Gosling, S. N., Hattermann, F., Hickler, T., Hinkel, J., Hof, C., Huber, V., Jagermeyr, J., Krysanova, V., Marce, R., Schmied, H.M., Mouratiadou, I., Pierson, D., Tittensor, D.P., Vautard, R., van Vliet, M., Biber, M.F., Betts, R.A., Bodirsky, B.L., Deryng, D., Frolking, S., Jones, C.D., Lotze, H.K., Lotze-Campen, H., Sahajpal, R., Thonicke, K., Tian, H., Yamagata, Y., 2017. Assessing the impacts of 1.5 degrees C global warming - simulation protocol of the Inter-Sectoral Impact Model Intercomparison Project (ISIMIP2b). Geosci. Model Dev. 10 (12), 4321–4345. https://doi.org/10.5194/gmd-10-4321-2017.

Fuchs, T., Rapp, J., Rubel, F., Rudolf, B., 2001. Correction of synoptic precipitation observations due to systematic measuring errors with special regard to precipitation phases. Phys. Chem. Earth Part B Hydrol. Oceans Atmosph. 26 (9), 689–693. https://doi.org/10.1016/S1464-1909(01)00070-3.

Gupta, H.V., Kling, H., Yilmaz, K.K., Martinez, G.F., 2009. Decomposition of the mean squared error and NSE performance criteria: implications for improving hydrological modelling. J. Hydrol. 377 (1–2), 80–91. https://doi.org/10.1016/j.jhydrol.2009.08.003.

Gu, X., Zhang, Q., Singh, V.P., Liu, L., 2016. Nonstationarity in the occurrence rate of floods in the Tarim River basin, China, and related impacts of climate indices. Glob. Planet. Chang. 142, 1–13.

Gu, X., Zhang, Q., Singh, V.P., Chen, Y.D., Shi, P., 2017. Temporal clustering of floods and impacts of climate indices in the Tarim River basin, China. Glob. Planet. Chang. 147, 12–24.

Jahandideh-Tehrani, M., Zhang, H., Helfer, F., Yu, Y., 2019. Review of climate change impacts on predicted river streamflow in tropical rivers. Environ. Monitor. Assess. 191 (12), 752. https://doi.org/10.1007/s10661-019-7841-1.

Knoben, W.J.M., Freer, J.E., Woods, R.A., 2019. Technical note: inherent benchmark or not? Comparing Nash–Sutcliffe and Kling–Gupta efficiency scores. Hydrol. Earth System Sci. 23 (10), 4323–4331. https://doi.org/10.5194/hess-23-4323-2019.

Kundzewicz, Z.W., Merz, B., Vorogushyn, S., Hartmann, H., Duethmann, D., Wortmann, M., Huang, S., Su, B., Jiang, T., Krysanova, V., 2015. Analysis of changes in climate and river discharge with focus on seasonal runoff predictability in the Aksu River Basin. Environ. Earth Sci. 73 (2SI), 501–516. https://doi.org/10.1007/s12665-014-3137-5.

Lenderink, G., Buishand, A., van Deursen, W., 2007. Estimates of future discharges of the river Rhine using two scenario methodologies: direct versus delta approach. Hydrol. Earth System Sci. 11 (3), 1143–1159.

Labat, D., Goddéris, Y., Probst, J.L., Guyot, J.L., 2004. Evidence for global runoff increase related to climate warming. Adv. Water Resour. 27, 631–642.

Li, X., Xu, C., Song Jia, L.L., Zhang, H., Bashir, A., 2019. Projection of future climate change in the Kaidu-Kongqi River Basin in the 21st century. Arid Zone Res. 36 (3), 556–566.

Liu, J., Zhang, W., Xia, J., Shen, Y., Kang, S., 2017. Study of degree-day model from 2000 to 2016: the main progress and key issues (in chinese). J. Glaciol. Geocryol. 39 (4), 801–810. https://doi.org/10.7522/j.issn.1000-0240.2017.0090.

Loh Y., W., 2002. Regression trees with unbiased variable selection and interaction detection. Statistica Sinica 12 (2), 361–386.

Luo, M., Meng, F., Liu, T., Duan, Y., Frankl, A., Kurban, A., De Maeyer, P., 2017. Multi–model ensemble approaches to assessment of effects of local climate change on water resources of the Hotan River Basin in Xinjiang, China. Water 9 (8), 584. https://doi.org/10.3390/w9080584.

Luo, Y.X., Xu, C.C., Chu, Z.C., Sun, Q., Chen, L., 2020. Application of CN05.1 meteorological data in watershed hydrological simulation: a case study in the upper reaches of Kaidu River basin. Clim. Chang. Res. 16 (3), 287–295.

Mamat, A., Wang, J., Ma, Y., 2021. Impacts of land-use change on ecosystem service value of mountain–oasis–desert ecosystem: a case study of Kaidu–Kongque River Basin, Northwest China. Sustainability 13, 140. https://doi.org/10.3390/su13010140.

McCabe, G., Clark, M., 2004. Trends and variability in snowmelt runoff in the Western United States. J. Hydrometeorol. 6 (4), 476–482.

Mccabe, G.J., Clark, M.P., 2005. Trends and variability in snowmelt runoff in the Western United States. J. Hydrometeorol. 6 (4), 476–482. ⟨http://www.jstor.org/stable/24910067⟩.

Moriasi, D.N., Arnold, J.G., Van Liew, M.W., Bingner, R.L., Harmel, R.D., Veith, T.L., 2007. Model evaluation guidelines for systematic quantification of accuracy in watershed simulations. Trans. ASABE 50 (3), 885–900. https://doi.org/10.13031/2013.23153.

Morton, F.I., 1983. Operational estimates of areal evapotranspiration and their significance to the science and practice of hydrology. J. Hydrol. 66 (1–4), 1–76. https://doi.org/10.1016/0022-1694(83)90177-4.

Moss, R.H., Edmonds, J.A., Hibbard, K.A., Manning, M.R., Rose, S.K., van Vuuren, D.P., Carter, T.R., Emori, S., Kainuma, M., Kram, T., Meehl, G.A., Mitchell, J.F.B., Nakicenovic, N., Riahi, K., Smith, S.J., Stouffer, R.J., Thomson, A.M., Weyant, J.P., Wilbanks, T.J., 2010. The next generation of scenarios for climate change research and assessment. Nature 463 (7282), 747–756. https://doi.org/10.1038/nature08823.

Najafi, M.R., Moradkhani, H., Jung, I.W., 2011. Assessing the uncertainties of hydrologic model selection in climate change impact studies. Hydrol. Process. 25 (18), 2814–2826. https://doi.org/10.1002/hyp.8043.

Nash, J.E., Sutcliffe, J.V., 1970. River flow forecasting through conceptual models part I — a discussion of principles. J. Hydrol. 10 (3), 282–290 http://doi.org/doi.org/10.1016/0022-1694(70)90255-6.
Nicodemus, K.K., Malley, J.D., Strobl, C., Ziegler, A., 2010. The behaviour of random forest permutation-based variable importance measures under predictor correlation. BMC Bioinform. 11 (1), 110. https://doi.org/10.1186/1471-2105-11-110.
Oudin, L., Michel, C., Anctil, F., 2005. Which potential evapotranspiration input for a lumped rainfall-runoff model? Part 1 - Can rainfall-runoff models effectively handle detailed potential evapotranspiration inputs? J. Hydrol. 303 (1–4), 275–289. https://doi.org/10.1016/j.jhydrol.2004.08.025.
Pachauri, R.K., Allen, M.R., Barros, V.R., Broome, J., Cramer, W., Christ, R., Church, J.A., Clarke, L., Dahe, Q.D., Dasqupta, P., Dubash, N.K., Edenhofer, O., Elgizouli, I., Field, C.B., Forster, P., Friedlingstein, P., Fuglestvedt, J., Gomez-Echeverri, L., Hallegatte, S., Hegerl, G., Howden, M., Jiang, K., Jimenez Cisneros, B., Kattsov, V., Lee, H., Mach, K.J., Marotzke, J., Mastrandrea, M.D., Meyer, L., Minx, J., Mulugetta, Y., Brien, K.O.T., Oppenheimer, M., Pereira, J.J., Pichs-Madruga, R.O.N., Plattner, G., Rtner, H.P.O., Power, S.B., Preston, B., Ravindranath, N.H., Reisinger, A., Riahi, K., Rusticucci, M., Scholes, R., Seyboth, K., Sokona, Y., Stavins, R., Stocker, T.F., Tschakert, P., van Vuuren, D., van Ypersele, J., 2014. Climate change 2014 synthesis report. contribution of working groups I, II, and III to the fifth assessment report of the Intergovernmental Panel on Climate Change. IPCC.
Perrin, C., Michel, C., Andreassian, V., 2003. Improvement of a parsimonious model for streamflow simulation. J. Hydrol. 279 (1–4), 275–289. https://doi.org/10.1016/S0022-1694(03)00225-7.
Poissant, D., Arsenault, R., Brissette, F., 2017. Impact of parameter set dimensionality and calibration procedures on streamflow prediction at ungauged catchments. J. Hydrol. Reg. Stud. 12, 220–237. https://doi.org/10.1016/j.ejrh.2017.05.005.
Pradhanang M., S., Mukundan, R., Schneiderman M., E., Zion S., M., Anandhi, A., Pierson C., D., Frei, A., Easton M., Z., Fuka, D., Steenhuis S., T., 2013. Streamflow responses to climate change: analysis of hydrologic indicators in a New York City water supply watershed. J. Am. Water Resour. Assoc. JAWRA 49 (6), 1308–1326. https://doi.org/10.1111/jawr.12086.
Rahnamay Naeini, M., Analui, B., Gupta, H., Duan, Q., Sorooshian, S., 2019. Three decades of the Shuffled Complex Evolution (SCE-UA) optimization algorithm: Review and applications. Scientia Iranica 26 (4), 2015–2031.
Riahi, K., Rao, S., Krey, V., Cho, C., Chirkov, V., Fischer, G., Kindermann, G., Nakicenovic, N., Rafaj, P., 2011. RCP 8.5-A scenario of comparatively high greenhouse gas emissions. Clim. Chang. 109 (1–2SI), 33–57. https://doi.org/10.1007/s10584-011-0149-y.
Santos, C.A.S., Rocha, F.A., Ramos, T.B., Alves, L.M., Mateus, M., de Oliveira, R.P., Neves, R., 2019. Using a hydrologic model to assess the performance of regional climate models in a semi-arid watershed in Brazil. Water 11 (1), 170. https://doi.org/10.3390/w11010170.
Shen, Y., Shen, Y., Fink, M., Kralisch, S., Chen, Y., Brenning, A., 2018. Trends and variability in streamflow and snowmelt runoff timing in the southern Tianshan Mountains. J. Hydrol. 557, 173–181. https://doi.org/10.1016/j.jhydrol.2017.12.035.
Sorg, A., Bolch, T., Stoffel, M., Solomina, O., Beniston, M., 2012. Climate change impacts on glaciers and runoff in Tien Shan (Central Asia). Nat. Clim. Chang. 2 (10), 725–731. https://doi.org/10.1038/NCLIMATE1592.
Sun, M., Yao, X., Li, Z., Zhang, M., 2015. Hydrological processes of glacier and snow melting and runoff in the Urumqi River source region, eastern Tianshan Mountains, China. J. Geogr. Sci. 25 (2), 149–164. https://doi.org/10.1007/s11442-015-1159-x.
Sun, P., Zhang, Q., Yao, R., Singh, V.P., Song, C., 2018. Low flow regimes of the Tarim River Basin, China: probabilistic behavior, causes and implications. Water 10 (470), 636–653. https://doi.org/10.3390/w10040470.
Thomson, A.M., Calvin, K.V., Smith, S.J., Kyle, G.P., Volke, A., Patel, P., Delgado-Arias, S., Bond-Lamberty, B., Wise, M.A., Clarke, L.E., Edmonds, J.A., 2011. RCP4.5: a pathway for stabilization of radiative forcing by 2100. Clim. Chang. 109 (1–2SI), 77–-94. https://doi.org/10.1007/s10584-011-0151-4.
Tian, L., Liu, T., Bao, A.M., Huang, Y., 2017. Application of CFSR precipitation dataset in hydrological model for arid mountainous area: a case study in the Kaidu River Basin. Arid Zone Res. 34 (4) https://doi.org/10.13866/j.azr.2017.04.06.
Troin, M., Arsenault, R., Martel, J., Brissette, F., 2018. Uncertainty of hydrological model components in climate change studies over two nordic quebec catchments. J. Hydrometeorol. 19 (1), 27–46. https://doi.org/10.1175/JHM-D-17-0002.1.
Troin, M., Arsenault, R., Brissette, F., 2015. Performance and uncertainty evaluation of snow models on snowmelt flow simulations over a nordic catchment (Mistassibi, Canada). Hydrology 2 (4), 289–317. https://doi.org/10.3390/hydrology2040289.
Turcotte, R., Fortin, L.G., Fortin, V., Fortin, J.P., Villeneuve, J.P., 2007. Operational analysis of the spatial distribution and the temporal evolution of the snowpack water equivalent in southern Québec, Canada. Hydrol. Res. 38 (3), 211–234. https://doi.org/10.2166/nh.2007.009.
Valéry, A., Andréassian, V., Perrin, C., 2010. Regionalization of precipitation and air temperature over high-altitude catchments – learning from outliers. Hydrol. Sci. J. 55 (6), 928–940. https://doi.org/10.1080/02626667.2010.504676.
Valéry, A., Andréassian, V., Perrin, C., 2014a. 'As simple as possible but not simpler': what is useful in a temperature-based snow-accounting routine? Part 1 – Comparison of six snow accounting routines on 380 catchments. J. Hydrol. 517, 1166–1175. https://doi.org/10.1016/j.jhydrol.2014.04.059.
Valéry, A., Andréassian, V., Perrin, C., 2014b. 'As simple as possible but not simpler': What is useful in a temperature-based snow-accounting routine? Part 2 – sensitivity analysis of the Cemaneige snow accounting routine on 380 catchments. J. Hydrol. 517, 1176–1187. https://doi.org/10.1016/j.jhydrol.2014.04.058.
van Vuuren, D.P., Stehfest, E., den Elzen, M.G.J., Kram, T., van Vliet, J., Deetman, S., Isaac, M., Goldewijk, K.K., Hof, A., Beltran, A.M., Oostenrijk, R., van Ruijven, B., 2011. RCP2.6: exploring the possibility to keep global mean temperature increase below 2 degrees C. Clim. Chang. 109 (1–2SI), 95–116. https://doi.org/10.1007/s10584-011-0152-3.
Velázquez, J.A., Troin, M., Caya, D., Brissette, F., 2015. Evaluating the time-invariance hypothesis of climate model bias correction: implications for hydrological impact studies. J. Hydrometeorol. 16 (5), 2013–2026 http://doi.org/doi.org/10.1175/JHM-D-14-0159.1.
Wang, R., Cheng, Q., Liu, L., Yan, C., Huang, G., 2019. Multi-model projections of climate change in different RCP scenarios in an Arid Inland Region, Northwest China. Water 11 (3472). https://doi.org/10.3390/w11020347.
Wang, X., Melesse, A.M., 2005. Evaluation of the swat model's snowmelt hydrology in a northwestern Minnesota watershed. Trans. ASAE 48 (4), 1359–1376.
Wang, Y., Xia, T., Shataer, R., Zhang, S., Li, Z., 2021. Analysis of characteristics and driving factors of land-use changes in the tarim river basin from 1990 to 2018. Sustainability 13, 10263. https://doi.org/10.3390/su131810263.
Wigmosta, M.S., Vail, L.W., Lettenmaier, D.P., 1994. A distributed hydrology-vegetation model for complex terrain. Water Resour. Res. 30 (6), 1665–1679. https://doi.org/10.1029/94WR00436.
Wu, J., Gao, X., 2013. A gridded daily observation dataset over China region and comparison with the other datasets. Chin. J. Geophys. Chin. Ed. 56 (4), 1102–1111. https://doi.org/10.6038/cjg20130406.
Yang, Y., Sun, H.W., Xue, J., Liu, Y., Liu, L.G., Yan, D., Gui, D.W., 2021. Estimating evapotranspiration by coupling Bayesian model averaging methods with machine learning algorithms. Environ. Monitor. Assess. 193 (3), 156. https://doi.org/10.1007/s10661-021-08934-1.
Yang, Z.L., Dickinson, R.E., Robock, A., Vinnikov, K.Y., 1997. Validation of the snow submodel of the biosphere-atmosphere transfer scheme with Russian snow cover and meteorological observational data. J. Clim. 10 (2), 353–373.
Yuan, F., Ma, M., Ren, L., Shen, H., Li, Y., Jiang, S., Yang, X., Zhao, C., Kong, H., W Ertsen, M., 2015. Possible future climate change impacts on the hydrological drought events in the Weihe River Basin, China. Adv. Meteorol. 2016, 2905198. https://doi.org/10.1155/2016/2905198.
Zampieri, M., Scoccimarro, E., Gualdi, S., Navarra, A., 2015. Observed shift towards earlier spring discharge in the main Alpine rivers. Sci. Total Environ. 503, 222–232. https://doi.org/10.1016/j.scitotenv.2014.06.036.
Zeng, L., Xiong, L., Liu, D., Chen, J., Kim, J., 2019. Improving parameter transferability of GR4J model under changing environments considering nonstationarity. Water 11 (10), 2029. https://doi.org/10.3390/w11102029.
Zhang, F., Bai, L., Li, L., Wang, Q., 2016a. Sensitivity of runoff to climatic variability in the northern and southern slopes of the Middle Tianshan Mountains, China. J. Arid Land 8 (5), 681–693. https://doi.org/10.1007/s40333-016-0015-x.
Zhang, F., Li, L., Ahmad, S., Li, X., 2014a. Using path analysis to identify the influence of climatic factors on spring peak flow dominated by snowmelt in an alpine watershed. J. Mt. Sci. 11 (4), 990–1000. https://doi.org/10.1007/s11629-013-2789-z.
Zhang, G.Q., Xie, H.J., Yao, T.D., Li, H.Y., Duan, S.Q., 2014b. Quantitative water resources assessment of Qinghai Lake basin using Snowmelt Runoff Model (SRM). J. Hydrol. 519, 976–987. https://doi.org/10.1016/j.jhydrol.2014.08.022.

Zhang, Q., Gu, Xi, Singh, V.P., Sun, P., Chen, X., Kong, D., 2016b. Magnitude, frequency and timing of floods in the Tarim River basin, China: changes, causes and implications. Glob. Planet. Chang. 139, 44–45.
Zhang, Y., Li, B., Bao, A., Zhou, C., Chen, X., Zhang, X., 2006. Simulation of snowmelt runoff in the Kaidu River Basin (in chinese). Chin. Sci. D Ser. Earth Sci. (24–32), S2–003 http://doi.org/CNKI：SUN：JDXK.0.2006.
Zhu, D., Das, S., Ren, Q., 2017. Hydrological appraisal of climate change impacts on the water resources of the Xijiang Basin, South China. Water 9 (10), 793 http://doi.org/doi.org/10.3390/w9100793.